Characterization of photocatalytic paints: a relationship between the photocatalytic properties – release of nanoparticles and volatile organic compounds

D. Truffier-Boutry, B. Fiorentino, V. Bartolomei, R. Soulas, O. Sicardy, A. Benayad, J.-F. Damlencourt, B. Pepin-Donat, C. Lombard, A. Gandolfo, et al.

Characterization of photocatalytic paints: A relationship between the photocatalytic property ï release of NanoParticles and Volatile Organic Compounds.

D. Truffier-Boutry[a], B. Fiorentino[a], V. Bartolomei[a,e], R. Soulas[a], O. Sicardy[a], A. Benayad[a], J-F Damlencourt[a], B. Pépin-Donat[b,c,d], C. Lombard[b,c,d], A.. Gandolfo[e], H. Wortham[e], G. Brochard[f], A. Audemard[f], L. Porcar[g], G. Gebel[a], S. Gligorovski[e,h*],*

[a] Université Grenoble Alpes, CEA, Laboratoire en Nanosécurité et Nanocaractérisation, 17 rue des Martyrs, F-38054 Grenoble Cedex 9, France

[b] Université Grenoble Alpes, INAC-SPRAM, F-38000 Grenoble France

[c] CNRS, INAC-SPRAM, F-38000 Grenoble, France,

[d] CEA, INAC-SPRAM, F-38000 Grenoble, France

[e] Aix Marseille Université, CNRS, LCE, UMR 7376, 13331, Marseille, France

[f] ALLIOS, Les docks Mogador, 105, chemin de St Menet aux Accates, F-13011 Marseille, France

[g] Institute Laue Langevin, Paul Langevin, BP 156, F-38042 Grenoble Cedex 9, France

[h] State Key Laboratory of Organic Geochemistry, Guangzhou Institute of Geochemistry, Chinese Academy of Sciences, Guangzhou 510 640, China

ABSTRACT

Photocatalytic TiO_2 appears to be a promising method to eliminate many air pollutants such as nitrogen oxides (NOx) and volatile organic compounds (VOCs). However, number of questions remain unanswered prior to their full optimization. Some photocatalytic materials are already commercialized but their photocatalytic effects are questionable. In the present study, a characterization of two paints for indoor and outdoor applications, one containing micro-size titanium dioxide (TiO_2) particles and the other based on nano-TiO_2, is undertaken in order to understand their environmental impact during the use phase. The photocatalytic efficiency of the paints is determined before and after climatic ageing. The degradation of the paints induced by their ageing was characterized in parallel. Powders, dispersions and paints applied on a substrate are investigated to characterize the state of the NanoParticles (NPs) as a function of their surrounding media. The abrasion of the photocatalytic materials indicates that the presence of TiO_2 (NPs) enhances the organic matrix degradation of the paints due to a greater photocatalytic effect. **The online and continuous measurements by PTR-ToF-MS indicate that the degradation of the organic matrix leads to release of organic compounds (formaldehyde, methanol, acetaldehyde and formic acid) in the air which suggests that following only the removal of VOCs (in this case xylene) is not enough to make a proper evaluation of the effectiveness of photocatalytic paints towards VOCs elimination. These VOCs emerge exclusively from the degradation of the organic matrix as much lower VOCs emissions were measured in the case of the aged paint which exhibits a lower amount of organic composition in the matrix.** This study links the morphological observations, chemical determination, structural parameters and photocatalytic properties of the paints for future optimization of a safer-by-design photocatalytic paints.

INTRODUCTION

In the construction industry, nanotechnology creates the possibility to produce materials with novel functionalities and improved characteristics. Products containing nanomaterials (NMs) have been developed for the construction sector[1] (cement, wet mortar and concrete, paints, coatings, insulation materials, glassé) because of their enhanced properties such as higher durability, fire resistance, thermal stability, self-cleaning and photocatalytic properties. Engineered Nanoparticles (ENPs), which by convention mean objects having at least one dimension within the nanometer range (1-100 nm), are more and more used in industrial applications. Different types of NPs are added in commercial paints to improve for instance their mechanical properties (SiO_2)[2], their UV resistance[3], their rheological properties[4] or to modify their coloring[5]. The industry associated with production of NPs takes into consideration a responsible development of its products[6]. This requires in particular a control of the NPs throughout the life cycle of the product. In this context, many toxicity studies are devoted to properly assess the impact of different types of NPs and their surrounding matrix, on human health[7]. Nevertheless, the best way to prevent inhalation and ingestion of NPs but also to avoid dermal contamination is to protect workers and consumers with appropriate equipment or to reduce the release of NPs in the environment. Therefore, some studies are more focused on the risk protection by studying collective[8, 9] and personal[10-13] protection systems while other studies investigate all the ways leading to reduce the release of the nanoparticles while maintaining their initial property (photocatalytic, antibacterial, reinforcement...)[14., 15].

A paint is generally composed of different components as binders, fillers, pigments, solvents, diluents and different additives like dispersing, thickeners and antifoam. The polymeric binder brings the adhesion to the substrate and the chemical resistance of the paint, fillers reduce cost and enhance the physical properties of paints and pigments provide the coloring to the paint. Titanium dioxide (TiO_2) particles with a micro-size are usually used as white pigment in paints.

When TiO_2 with nano-range size are embedded in the paint, the coloring property is lost but these NPs provide a photocatalytic effect reducing air contaminants such as NOx and VOCs in the environment to indoor and outdoor construction materials[16-19] (concrete, asphalt, tiles, paintsé). Regarding the outdoor applications, the TiO_2 NPs were used to attempt to reduce the adverse effects of urban air pollution on human health. Titanium dioxide (TiO_2) based photocatalytic surfaces have been tested, both, at a laboratory scale and in the real-life urban environment for the remediation of Nitrogen Oxides (NOx), Volatile Organic Compounds (VOCs) Ozone (O_3) and atmospheric particles. The results of these studies are controversial and the reasons for these contradictory results are still under discussion suggesting that further studies are necessary in order to accurately determine the impact of photocatalytic materials on air quality. Few studies have demonstrated that instead of VOCs elimination, the emission of carbonyl compounds occurs during the irradiation of the photocatalytic paints. For example, **Gunschera *et al.*[20] identified emissions from building materials as formaldehyde, furfural, acetophenone, n-butylbutyrate, n-butyl-i-butyrate, n-butylpropionate, 4-heptanone, acetic acid, i-butyraldehyde and crotonaldehyde, in the case of photocatalytic tiles.** The release of harmful aldehydes such as formaldehyde, acetaldehyde, 2-ethylacrylaldehyde, pentanaldehyde, and hexanaldehyde was observed upon irradiation of photocatalytic paints[21]. Another controversial issue is the potential formation of by-products such as nitrous acid (HONO)[22], which is even more harmful than the primary reactants NO and NO_2. Regarding the indoor application of photocatalytic paints, Gandolfo *et al.*[23] have shown that HONO is released in the indoor air in function of the embedded quantity of TiO_2 nanoparticles.

In parallel, other studies are more focused on the possible release of TiO_2 NPs in the environment during the use phase of the photocatalytic paints. Al Kattan *et al.*[24-25] studied the TiO_2 NPs release from paints before and after climatic ageing and also their behavior when exposed to different media (pH and different organic matters). Olabarrieta *et al.*[26] immersed the

98 photocatalytic paints in different media during UV irradiation. Shandilya *et al.*[27] investigated
99 the emission of TiO_2 NPs during ageing in water with the analysis of the run-off and in the air
100 via abrasion experiments. All stated that the photocatalytic effect initiated by UV-light degrades
101 the organic matrix of the paints and increases the release of NPs to the environment.

102 The present paper links both NPs and VOCs release in the environment during the ageing of a
103 photocatalytic paint. The aim of the study consists in a better understanding of the main
104 parameters controlling the release of NPs from nanomaterials in order to formulate, in the
105 future, safer-by-design paints i.e. less NPs and VOCs releasing paints with the same
106 photocatalytic efficiency. For this purpose, two different paints were investigated. Both paints
107 exhibit the same formulation, but they differ by the amount and size (micro and nano) of the
108 TiO_2 particles. The paint containing micro-TiO_2 is already commercialized, and the one with
109 the nano-TiO_2 is still under development. The use phase of these two products was investigated
110 by simulating environmental and mechanical ageing.

111 TiO_2 powders, dispersions and paints applied on a substrate were characterized to determine
112 the chemical nature, the particle size distribution, the particle shape and the dispersion state. In
113 a second phase, outdoor ageing of the products was simulated: painted panels were exposed to
114 accelerated weathering. The photocatalysis property of TiO_2 powders and applied paints was
115 investigated by EPR (Electron Paramagnetic Resonance) and the photocatalytic activity was
116 measured with an HR PTR ToF MS (High Resolution Proton Transfer Reaction Time of Flight
117 Mass Spectrometry) before and after ageing to correlate with the surface characterization. All
118 these technics allowed to perform the analysis of the surface and the bulk of each sample. It
119 facilitated the understanding of the weathering effect on paints, of its impact on NPs release
120 and on the interaction between the polymeric binder and pigments. Abrasion tests were
121 performed with a Taber abraser to simulate a mechanically induced ageing.

122

MATERIALS AND METHODS

Preparation of the paints

All the analyzed samples were provided by the same manufacturer ALLIOS. Two types of paints were investigated. Both paints were composed of the same constituents in the same proportion such as an acrylic-based binder, inactive microsize TiO_2 for the white color, calcium carbonate particles, aluminosilicate, water and other additives, called ñbasic paintò. Their formulation differed only by the size of TiO_2 particles used. For the formulation of the photocatalytic paint, a slurry was at first made. The D2 slurry was composed of TiO_2 NPs called P2 in anatase form and the D1 slurry was composed of inactive TiO_2 microsize particles called P1. Both slurries D1 and D2 contained of about 70% (w/w) of P1 and P2 TiO_2 respectively in water. About 5% (w/w) of D1 and D2 slurries were mixed with the ñbasic paintò to reach 2.5% (w/w) of P1 and P2 in PM1 paint (for Matte Paint 1) and PM2 paint (Matte Paint 2). PM1 and PM2 were both investigated to compare a non-reactive paint with a reactive one. The manufacturer provided powders, dispersions, liquid paints and also paints applied on different substrates allowing us to perform various experiments and characterizations.

TiO_2 powders (P1 and P2) were characterized by X-Ray Diffraction (XRD, Bruker-advance diffractometer), by Scanning Electron Microscopy coupled with an Energy Dispersive X-ray spectrometer (SEM-EDX, LEO Electron Microscopy Ltd, Quantas EDX, Bruker Nano), by Transmission Electron Microscopy coupled with an Energy Dispersive X-ray spectrometer (TEM-EDS, FEI Tecnai Osiris) and by X-Ray Photoelectron Spectroscopy (XPS, PHI Versa Probe II spectrometer). As the P2 NPs are agglomerated in the powder state, they were characterized in solution by cryo high resolution-transmission electron microscopy (cryo HR-TEM, FEI Tecnai Osiris). Dispersions D1 composed of about 70 weight % of P1 microparticles in water and dispersion D2 composed of about 70 weight % of P2 nanoparticles in water were

also investigated since the manufacturer use these dispersions to formulate the paints. Small-Angle X-Ray Scattering (SAXS) and Small-Angle Neutron Scattering (SANS) were used to determine the real size and the structure of the P2 NPs in the dispersed state. These techniques were chosen because they provide results which are more representative of the samples compared to TEM observations. Paints applied on Leneta plastic substrates (black plastic-vinyl chloride/acetate copolymer with smooth matte surface, thickness of 0.25 mm and size of 165 x 432 mm) were characterized by SEM-EDS and XPS before and after accelerated weathering. The photocatalytic property was measured by EPR (EMX Bruker spectrometer) on powders and applied paints under solar simulation (New Port Oriel, Sol 3A class AAA solar simulator 94023A). A Proton Transfer Reaction-Time of Flight-Mass Spectrometer (PTR-ToF-MS) (Ionicon) was connected to a sealed reactor during the injection of a VOC on painted surfaces stored during 21 days in an oven ventilated by clean air at 23°C and 55 % relative before to evaluate their photocatalytic efficiency with respect to xylene. Paints applied on metallic substrates (Taber industries aluminum panels of 100mm^2 with a 6.35 mm center hole) were used for abrasion tests (Taber Abraser (type 5131, Taber Industries) before and after accelerated weathering in a QUV climatic chamber (Q-Lab, USA).

Photocatalytic efficiency.

The photocatalytic effect was measured before and after accelerated weathering of both paints. For these measurements, paint samples are placed in a flow tube rector and exposed to VOCs. For details about the working principle of the flow tube reactor the readers are referred to Gandolfo *et al.*[19, 23]. The flow tube reactor is coupled to a PTR-ToF-MS for on-line and continuous measurements of the variations of the concentrations of VOCs. This system is very sensitive for real-time monitoring of VOCs present in the air (acetone, acetaldehyde, methanol, ethanol, benzene, toluene, xylene among the others). Two types of experiments were conducted,

(i) following the concentrations of all the released VOCs from the samples upon light irradiation and (ii) following the removal of one selected VOCs (xylene) due to the photocatalytic efficiency of the paint. We have chosen to monitor the elimination of xylene by photocatalytic paints because it is considered toxic for humans[28], it is not emitted in the air by paints and it is present in non-negligible concentrations in indoor atmospheres[29] because some materials generate this compound[30].

Photocatalytic property measured by EPR. EPR spectra were obtained at 9 GHz at room temperature. Samples were observed either wetted or with pure 5,5-dimethyl-1-pyrroline N-oxide (DMPO) used as ñspin trapò. It consists in trapping radicals that are extremely difficult to be observed because of their short life time, by a diamagnetic molecule in order to obtain a stable paramagnetic species. The spin trapping technique involves the addition of the unstable radical to the double bond of a diamagnetic spin trap. This technique allows the identification of the nature of the unstable trapped radical. Such analyses were performed in dark or under 15 min light irradiation with a solar simulator to characterize the photocatalytic property of the paints. For irradiation tests, samples were placed in a fixed position located at 5 cm below the device producing the photons from the solar simulator. In this way, the center of the solar simulator coincide with the center of the sample. The EPR spectra were recorded under Ar atmosphere after air exchange inside a glovebox in order to avoid broadening of the line widths due to the presence of oxygen.

Ageing: Q-UV exposure conditions. Paint coated panels (Leneta and aluminum) were exposed to UV lamps in an accelerated weathering chamber for 500 hrs according to the ISO norm 16474-3:2013 (ISO 2013). The applied lamp is a Fluorescent UVB 313 and the UV light was emitted in the wavelengths range from 290 nm to 400 nm with a maximum applied irradiance

of 0.71 w m^{-2} at 310 nm. Paints underwent two different cycles: a) 5hrs with lamps switched on at a temperature of 50±2 °C and b) 1hr with lamps switched off with a water spray at a temperature of 25±2 °C. Exposed paints to UV lamps were noted ñQUVò. The total radiance exposure was 1.44 MJ m^{-2} giving a maximum acceleration using short wavelength UV.

X-Ray Diffraction (XRD). The crystallographic structure of nanoparticles was investigated using a Bruker-advance diffractometer in geometry θ-2θ, equipped with a Cu-Kα source and a LynxEye linear detector. θ-2θ patterns were achieved in order to identify the various crystallographic phases and precisely measure their lattice parameters.

Small-angle scattering: Small-Angle Neutron Scattering (SANS) experiments were performed on the D22 spectrometer of the Institut Laue-Langevin (ILL, Grenoble). Three different configurations (incident wavelength, λ and sample-to-detector distance) were used to cover a transfer momentum range from 3.10^{-3} and 0.5 $Å^{-1}$, q (where $q=4\pi \sin\theta/\lambda$ and θ is the scattering angle). Small-Angle X-ray Scattering (SAXS) experiments were performed on the D2AM beamline of the European Synchrotron Radiation Facility (ESRF, Grenoble). Both dispersions D1 and D2 were studied in liquid cells with quartz and Kapton windows for SANS and SAXS, respectively. Usual corrections for intensity normalization and background subtraction were applied[31].

Scanning Electron Microscopy coupled with an Energy Dispersive X-ray Spectrometer (SEM-EDS). Images were acquired with an ultra-High Resolution SEM (HR-SEM). Samples were covered by a 10nm layer of platinum to prevent charging during observations. For the acquisition of images, the working distance was less than 4mm with an accelerating voltage of 5kV and a diaphragm of 30μm. EDS analysis were performed to obtain chemical information

on observed samples. The quantification of EDS spectra was done using the ñESPRITò software, allowing an accurate chemical elemental analysis. For this, the working distance and the accelerating voltage were raised to 8mm and 15kV respectively, with a diaphragm of 60µm. SEM-EDS allowed us to characterize powders and paint samples applied on Leneta substrates before and after ageing.

Transmission Electron Microscopy coupled with an Energy Dispersive X-ray Spectrometer (TEM-EDS). TEM samples were prepared by simple drying of a drop of the sonicated solution on a carbon film grid. This analytical system owns four EDX detector giving a solid angle close to 1 steradian. Analysis were carried out in STEM mode using the HAADF (High Angle Annular Dark Field) detector at a high voltage of 200 kV with a probe current of 0.4 nA. Probe size was approximately 5 angstrom. Cryo-preparation was carried out using a Vitrobot plunger in liquid ethane. After sonication, a drop of the solution was deposed on a C-FLAT carbon grid and freeze at ethane temperature. Observations were made using a single tilt Gatan cryo holder working at liquid nitrogen temperature. Images were recorded using low-dose mode at 200 kV (dose reduced to 10 e-.A.s-1) with a Gatan BM-Ultrascan camera equipped with a biological scintillator.

X-Ray Photoelectron Spectroscopy (XPS). XPS allowed us to determine the surrounding environment of elements present at the near surface of samples (first 10 nm).The XPS measurements were performed using spectrometer with a monochromatized Al KŬ X-ray source (1486.6 eV) focalized to a spot of 100 µm and with an electron take-off angle of θ = 45°. Survey spectra were recorded with a pass energy of 117 eV and the high-resolution spectra were registered with a pass energy of 23.5 eV. Known as non-destructive surface analysis

instrument, XPS allowed us to probe the chemical bonds and their evolution after climatic ageing.

Abrasion process. All manipulations were performed in a so-called low noise glove box equipped with an HEPA filter in order to limit the initial presence of particles in the atmosphere[32]. The background noise in the sealed glove box was quantified by a Condensation Particle Counter (CPC) to be less than 5 particles cm^{-3}. This particular condition was achieved by creating a vacuum which sucks the air at a rate of 150 l min^{-1} at the top of the box. A clean air was obtained using a filter placed at the bottom of the glove box. For the abrasion of the surface paints, a Taber Abraser was used. This test simulated the ageing effect induced by a mechanical friction. A S42 abrasive sticker paper was set on CS-0 wheel to simulate the sanding process of a surface. A weight of 500g was applied on both wheels of the Taber during 100 cycles of rotary abrasion at 60rpm. These abrasion conditions are conforming the standard ISO 7784-2 (ISO 2006).

The characterization of the released particles due to the abrasion process was obtained by the determination of the particle size distribution with an Electrical Low Pressure Impactor (ELPI) (DEKATI ltd, Tampere, Finland). The ELPI allowed to collect aerosolized particles according to their aerodynamic diameter on hydrophilic polycarbonate membranes containing holes of 100 nm. Both membranes located in the two last impactor stages of the ELPI column, corresponding to the smallest particles size impaction (of about 10nm), were then analyzed by SEM-EDS. The goal was to observe the morphology and the size, and also to determine the elemental analysis of the collected nanoparticles.

RESULTS

Characterization of pristine particles P1 and P2. Pristine particles were observed by microscopy (SEM and TEM), chemical identification was conducted by EDS and their crystalline structure were determined by XRD. As seen on Figure 1, particles P1 had an elongated shape and their size was of about 240nm in length and 150nm in width. P2 particles were aggregated, forming pellets with size above 200nm as observed by SEM. TEM-EDS observations show that P1 particles were coated with a thin layer of carbon. To better observe P2 NPs, a cryo-HR-TEM was used to observe a solution composed of P2 NPs and water in a frozen state. Isolated NPs with an average diameter of about 5nm were observed.

EDS measurements identified predominantly titanium and oxygen for both powders. XRD measurements reveal that P1 is mainly composed of particles having a rutile crystalline structure and a minor crystallite structure anatase phase. On the other hand, P2 has only an anatase crystalline structure.

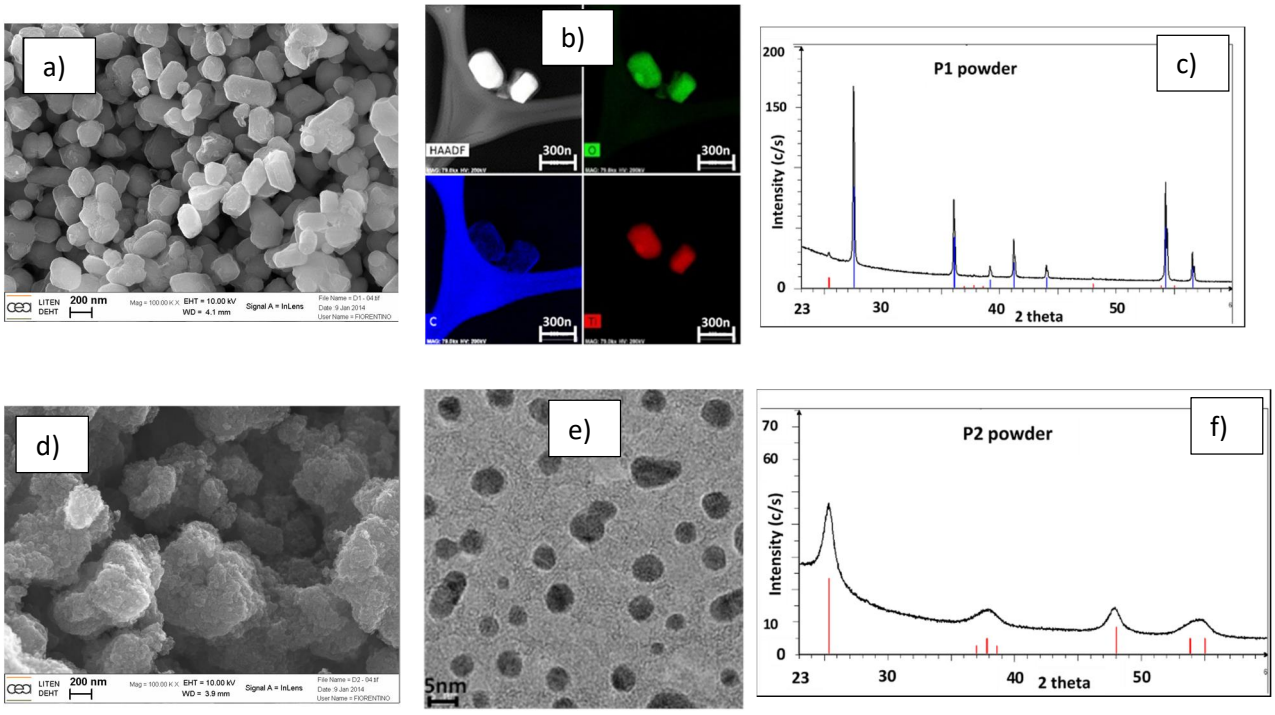

Figure 1: a) SEM micrograph, b) TEM micrograph, c) XRD measurement of pristine P1 microparticles. d) SEM micrograph, b) HR cryo-TEM micrograph, c) XRD measurement of pristine P2 nanoparticles.

Characterization of P1 and P2 dispersions: The structure of P1 and P2 dispersions were studied by SANS and SAXS. The spectra are presented on Figure 2. A scaling factor, the same for both P1 and P2, was applied to the SAXS data to superimpose with SANS results. The scattered intensity varies over 8 orders of magnitudes. The spectra obtained with the D1 and D2 dispersions are very different on the overall angular range. The D1 spectra vary as q^{-4} as expected for large size particles according to the Porodôs law. The deviation observed at large angles is significant and cannot be eliminated, modifying the background subtraction. The D2 spectra appear strongly different with a q^{-3} upturn in intensity at low angles, characteristic of aggregated particles with a strong dispersion in the aggregation number and an oscillation around 0.1 $Å^{-1}$ that should originate from particles with a size around 5nm. The SANS and SAXS data for both dispersions are exactly superimposable at low angles. The contrast for X-rays is directly related to the very large electron density difference of TiO_2 compared to water while Ti presents a negative scattering length enhancing the contribution of a carbon shell. But interestingly, the spectra do not match anymore at large angles, revealing a non-homogeneous structure. Based on the characterization results presented above, the spectra were fitted with a core-shell model assuming spherical particles with a TiO_2 core surrounded by a thin carbon shell for calculating the scattering length densities with a Gaussian polydispersity of 0.35. The same particle core diameter and shell thickness were used to adjust the SAXS and SANS spectra. For D1, a value of 150nm was chosen for the core radius because this value cannot be adjusted due to the large size of the particles. The shell thickness is 0.6 nm. For D2, the core radius is 1.2nm and the shell was found to be very thin (0.16nm) which indicates that it cannot

be undoubtedly identified by TEM or XPS characterizations. The possible reason for this could be the carbon contamination of the TiO_2 NPs. The signal scattered at low angles for D2 originates from aggregated particles with a fractal structure, the contribution of which is not encountered in the model. Comparing the level of intensities between the upturn in intensity and form factor of the nanoparticles, it can be estimated that less than 10% of the nanoparticles are aggregated in agreement with cryo-TEM observations in Figure 1e).

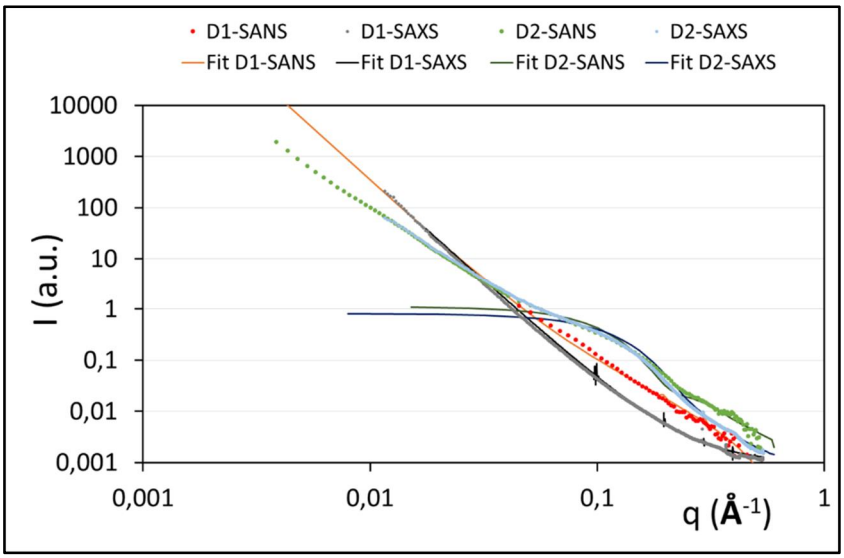

Figure 2: SANS and SAXS profiles of D1 and D2 dispersions as a function of the scattering-vector modulus *q* and their respective theoretical simulations.

Surface characterization of applied paints PM1 and PM2 before and after ageing. PM1 and PM2 were applied on Leneta substrate (polymer substrates). SEM images of the paintsô surface before and after the QUV ageing are shown in Figure 3 at different scales (X1000, X10000, X100000). At each scale, differences were observed between aged and non-aged paints. By focusing at the largest scale (X100 000) before ageing, it could be seen that P1 and P2 particles were covered by a thin layer of organic matrix. After ageing, the organic layer had disappeared, P1 and P2 were found at the surface of samples. For PM1, a dense layer of P1 is

observed after ageing. In the case of PM2 sample, not only P2 particles, but also the plastic substrate, was observed at the surface.

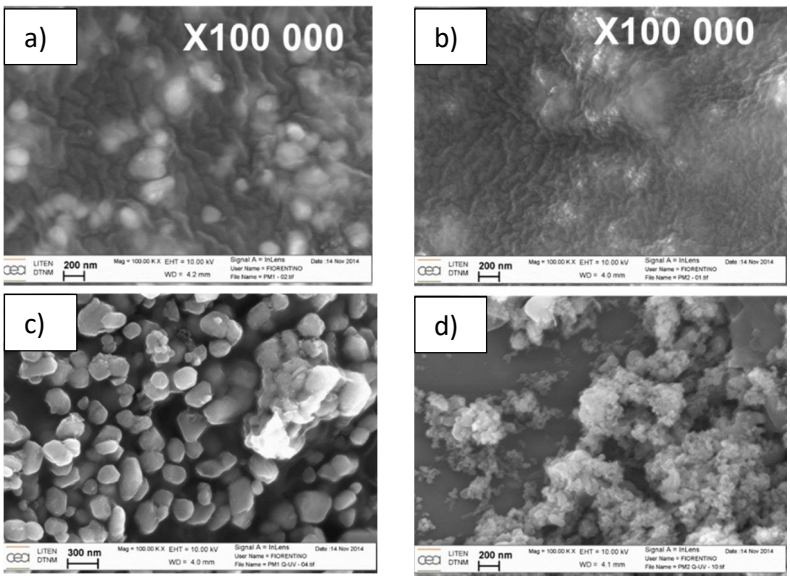

Figure 3: SEM images of a) PM1, c) PM1 Q-UV, b) PM2, d) PM2 Q-UV at X100 000 scale.

To better understand the effects emerging from the ageing of both paints, XPS measurements were performed before and after ageing (Figure 4). The XPS C 1s core peak registered at the surface of PM1 and PM2 samples before ageing (in black on Figure 4) was the signature of species related to the organic matrix for instance C-C/C-H at (284.8 eV), C-O at (286.3 eV), COO at (289.0 eV) and CO_3 bonds related to $CaCO_3$. The O 1s core peak corroborated this effect by the presence of a main peak at (532.4 eV) related to acrylic and vinyl copolymer. The Ti 2p core peak was not detected before ageing in the case of both paints, indicating that the organic layer (observed by SEM on Figure 1) covering the surface of TiO_2 particles was thicker than 5 nm.

After ageing (in red on Figure 4), the intensity of the C-O and C-C related peaks at the C 1s peak decreased and simultaneously the O 1s showed the appearance of a shoulder at 530 eV

assigned to TiO_2 particles. The valence state of TiO_2 particles was probed by the mean of Ti 2p peak indicating the presence of +4 oxidation state of titanium (peak at 458.6 eV).

In the case of PM2 paint, qualitatively a similar behavior was observed. However, some differences were observed quantitatively. Before ageing, the amount of C-O was lower .The ratio O [O^{2-}]/O[organic] before and after UV exposure was evaluated for both samples, and reported to be 0 and 0.42 in the case of PM1 and 0 and 2.08 for PM2 sample.

In the case of PM2 paint, the higher intensity of Ti^{4+} and of O^{2-} peaks registered after ageing was related to the presence of mainly P2 TiO_2 nanoparticles at the extreme surface of the sample. In parallel, the polymer matrix degradation was observed with the decrease of the C-O-related peak of the C1s spectrum.

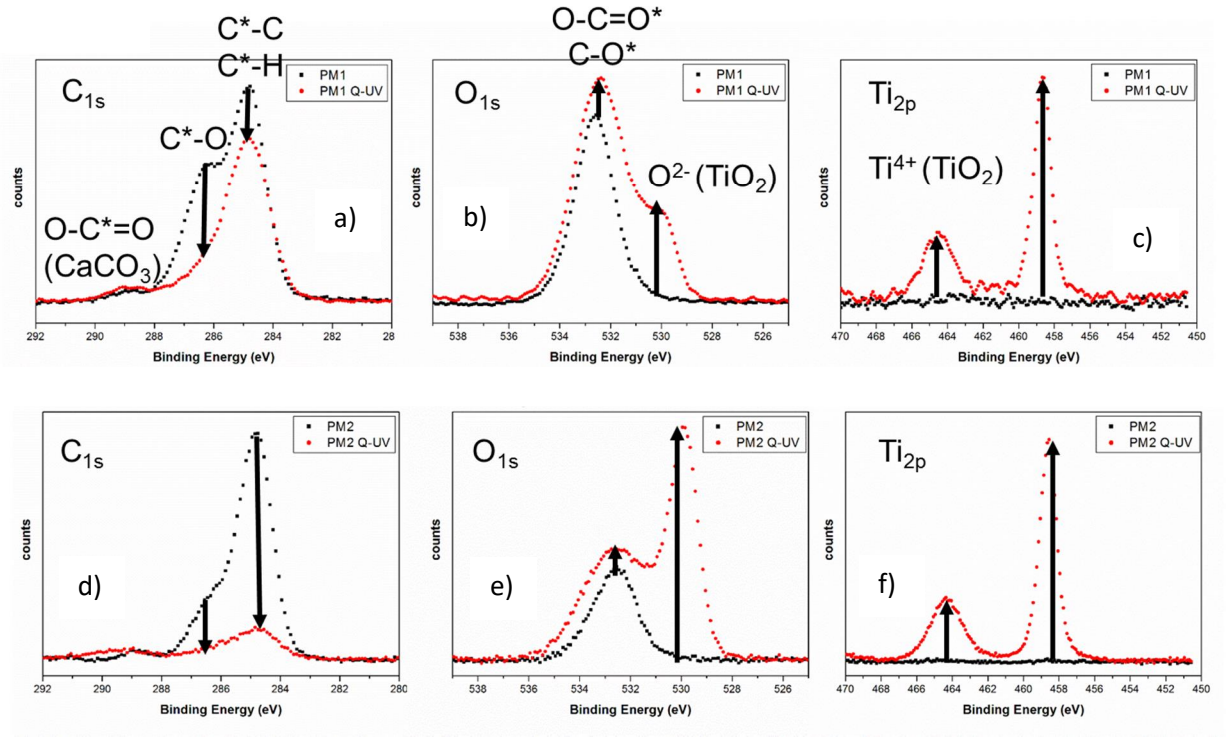

Figure 4: XPS spectra of PM1 and PM2 before and after ageing. a) C1s, b) O1s, c) Ti2p core level spectra of PM1 and d) C1s, e) O1s, f) Ti2p core level spectra of PM2.

Aerosolized particlesô characterization. Particle size distributions analyzed by ELPI counter during ongoing abrasion process are depicted in Figure 5. This type of counter measured the particle diameter as a function of their aerodynamic diameter (ranging from 7 nm to 10 µm). It was observed that all the non-aged paints released less particles than the aged paint containing nanoTiO_2 (PM2).

Aged PM2 sample released mostly NPs with diameter smaller than 100nm. NPs impacted on the last stage of the ELPI column were observed by SEM-EDX and were found to be TiO_2 NPs.

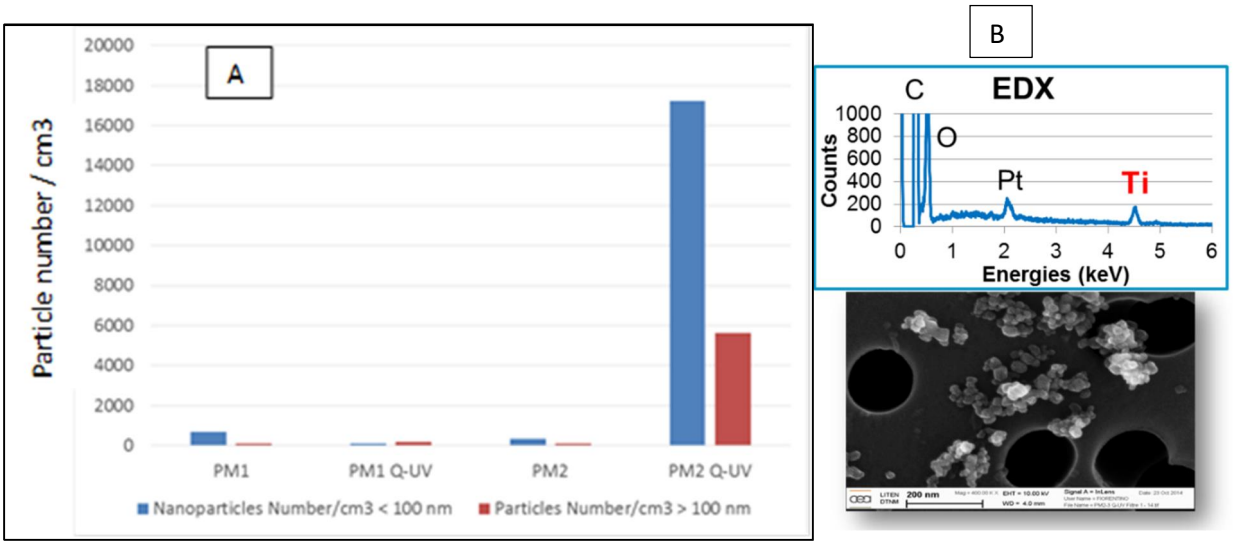

Figure 5: A) Concentration of particles released as a function of the particle size measured with ELPI; B) SEM-EDS characterization of the released particles.

Test of the photocatalytic performance. Signals provided by both powders with and without solar simulation have been recorded and are gathered in Figure 6a). Since the considered photocatalytic paints in this study absorb in the visible range of wavelengths, even in absence of solar light irradiation (only presence of ambient light), both TiO_2 powders give EPR signals. The light irradiance supplied by the lamps present in the room is sufficient to shift the electron of the valence band towards the conduction band forming an electronic dipole (electron / electron hole). The electron (e^-) and the electronic hole (h^+) react with gas, such as molecular

oxygen (O_2) and water vapor (H_2O) adsorbed on the semiconductor surface (TiO_2). The formation of these hole-electron pairs creates highly reactive species such as hydroxyl radicals ($^{\bullet}OH$), superoxide radical ($^{\bullet}O_2^-$) and hydrogen peroxide radical ($^{\bullet}OOH$) that oxidize organic compounds which are adsorbed on the surface of the catalyst[33]. The EPR signal is composed of three lines with respective g-factor of 2.023, 2.009 and 2.004 which can be interpreted in two ways: either to the $Ti^{4+}O^{2-}Ti^{4+}OH^{-\bullet}$ species[34-38] or to oxygenated radicals[39] due to photoreaction of residual organic groups as reported for cysteine-modified TiO_2 colloids[37, 40] ascribed to TiO_2 reactivity. The broad signal observed at higher g-value (between 2.08 and 2.06) may be likely ascribed to $^{\bullet}O_2^-$ adsorbed on the nanoparticle surface[41]. At lower g value (g=1.96), we did not observe the signal corresponding to electrons[42], which could possibly be attributed to the difference between the temperature of observation, 10K in our case against 4K in the study by Kumar *et al.*[42]. Both signals of nano and micro TiO_2 particles spectra look very similar, except for the first line (higher g value) for microTiO_2 which appears at slightly higher g-factor compared to nanoTiO_2 (2.035 against 2.026)[42]. Under solar simulation, signals are more intense for both powders. However, nanoTiO_2 powder was the most reactive (in dashed grey line) and showed higher intensity signals.

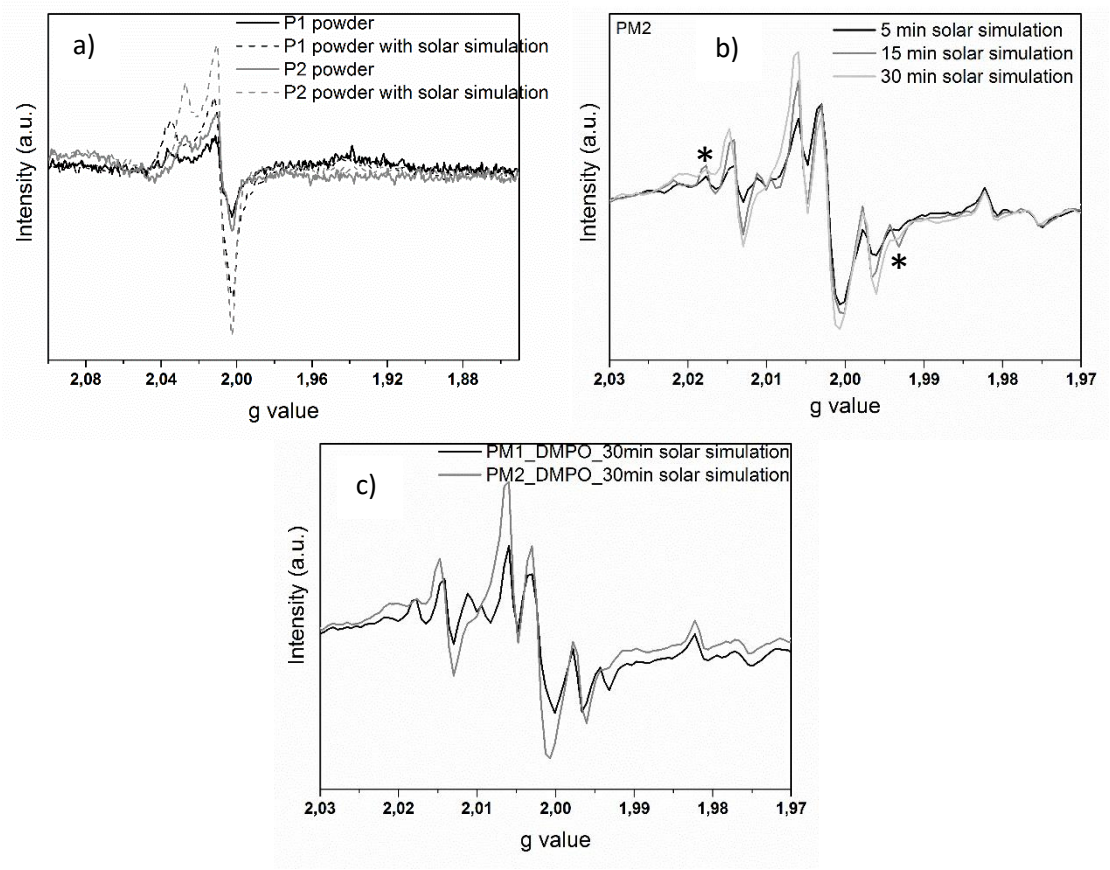

Figure 6: EPR signals of a) microTiO_2 P1 and nanoTiO_2 P2 powders with and without solar irradiation, b) PM2 paint applied on Leneta substrates with DMPO in function of the duration of the solar irradiation and c) PM1 and PM2 applied on Leneta substrate with DMPO both after 30min of solar irradiation.

EPR experiments were also conducted on paints applied on Leneta substrates in the presence and absence of solar irradiation, Figure 6b and c). In order to observe the various radical species involved during the TiO_2 catalysis photoreaction, we have applied the so-called ñspin trapping methodò. The unstable free radical reacts with DMPO and forms a relatively stable nitroxyl radical exhibiting very distinguishable EPR spectra. When the paints which were in contact with pure DMPO were illuminated, new lines appeared which varied with the irradiation time (Figure 6b). The separation in Gauss between the two extreme lines which appears (*) upon

illumination is on the order of 42 Gauss. This fits well with hyperfine coupling expected in the case of trapped •OH radical. Even embedded in a paint formulation, TiO_2 reacts and generates •OH radicals at the sample surface or within the paint coat for both paints PM1 and PM2 as shown in Figure 6c. The formation of •OH radicals upon illumination of TiO_2 and polyacrilonitrile is well known mechanism and already observed[43, 44].

The photocatalytic performance of the paints was investigated, as well. In this sense, two types of experiments were performed, i) on-line analysis of VOCs released by the paints upon light irradiation and ii) on-line monitoring of the removal of xylene induced by the photocatalytic effect of the paints. All the VOCs released from pristine and aged PM1 and PM2 paints are observed on Figure 7. Four types of VOCs appeared in the reactor under illumination of the paints: formaldehyde (m/z 31), methanol (m/z 33), acetaldehyde (m/z 45) and formic acid (m/z 47). At first glance, it can be seen that PM2 paint released a bigger amount of VOCs compared to PM1, especially for non-aged samples. Thus, although these photocatalytic materials are aimed to eliminate a broad range of volatile organic compounds, they release harmful pollutants, such as formaldehyde, for instance. These observations are in agreement with the literature data. For example, the release of formaldehyde was also observed upon light irradiation of photocatalytic paints by Salthammer and Fuhrmann[21].

Concerning the removal of xylene induced by the photocatalytic activity of both paints, the first order rates of xylene disappearance were measured. The PM1 paint was not able to eliminate xylene; hence, it was impossible to measure the corresponding rate constant. On the other hand, first order rate constant of (9.5 ± 4.5) Ā10^{-4} s^{-1} was measured for pristine PM2 and (5.7 ± 0.9) Ā10^{-2} s^{-1} for the aged PM2. Hence, the aged paint containing nano-TiO_2 was much more effective (ca. two orders of magnitude) in terms of photocatalytic removal efficiency towards xylene.

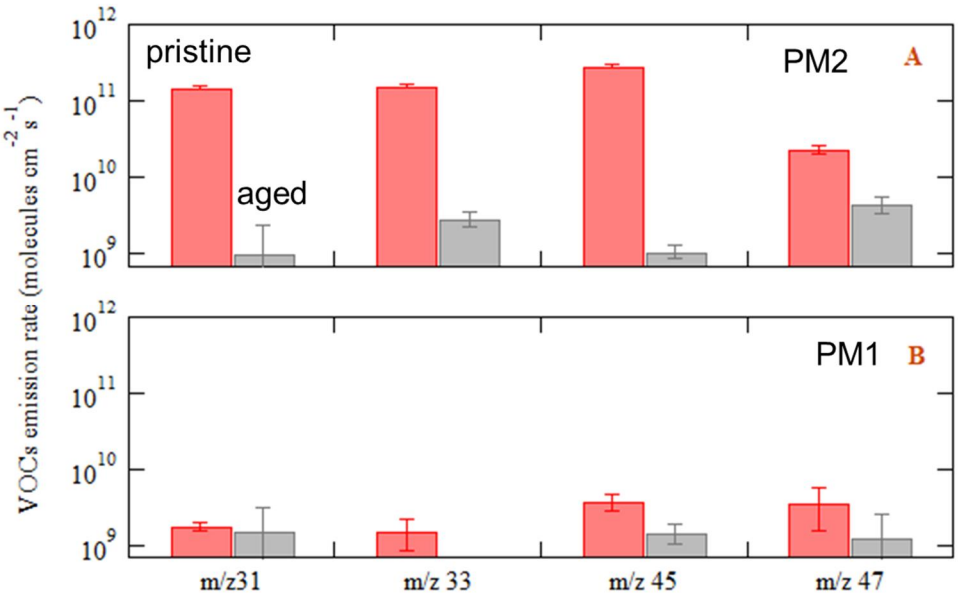

Figure 7: Surface emission rates of released VOCs for both PM1 and PM2 paints, pristine and aged ones.

DISCUSSION

Nano-TiO_2 is known for its photocatalytic property. Manufacturers add it in their formulation for their VOCs removal action. In this study, we reveal that the paint containing TiO_2 particles with sizes up to 100nm and rutile crystalline structure (PM1) cannot remove xylene from the air, independently of its aging state, as the decay of xylene could not be measured (see Figure 2 in the supplementary information). On the other hand, the paint composed of TiO_2 NPs with anatase crystalline structure enables the degradation of xylene as the first order decay of xylene were (9.5 ± 4.5) Ā10^{-4} s^{-1} and (5.7 ± 0.9) Ā10^{-2} s^{-1} for non-aged and aged PM2 paints, respectively. While the photocatalytic properties of the paint improves the elimination of VOCs such as xylene, it leads also to the generation of four additional VOCs that are released in the environment at the same time. Among the four identified compounds, formaldehyde **which is a sensory irritant**, has been classified as carcinogenic substance[45]. The benefit of the photocatalytic property to clean up the environment is counterbalanced by the emission of harmful VOCs and also by the possible release of NPs. Indeed, a high amount of NPs,

519 essentially composed of Titanium, was observed on the EDX spectrum (Figure 5b), released by
520 the aged PM2. Despite the fact that the same free radicals are generated during EPR experiments
521 of P1 and P2 powders, three lines with respective g-factors of 2.023, 2.009 and 2.004 related to
522 TiO_2 reactivity, P2 nanoparticles with anatase crystalline structure are more efficient than the
523 rutile microparticles. If the EPR peak intensities of P1 and P2 are similar when non-irradiated,
524 P2 EPR spectrum showed more intense peaks compared to P1 under UV-irradiation. P1 does
525 not act as VOCs removal agent contrary to P2 which exhibits a high reactivity under UV-
526 radiation, in agreement with the literature data[46, 47]. A possible explanation could be that the
527 anatase crystalline structure exhibits lower recombination rates combined with higher surface
528 adsorptive capacity with organic compounds[48], leading to production of more free radicals
529 acting on VOCs. When P1 and P2 are added in a paint (so called PM1 and PM2 formulations),
530 EPR spectra show more peaks attributed to trapped •OH radicals (Figure 6 c) generated at the
531 paint surface or within the paint[44] which are responsible of the VOCs degradation. As observed
532 for irradiated P1 and P2, PM2 show more intense EPR peaks and the amount of generated •OH
533 radicals increases with the irradiated time (see Figure 6 b), confirming that nano-TiO_2 based
534 paint PM2 is indeed more reactive than PM1. Concerning the crystalline structures, it is well-
535 known that these two principal structures exhibit different photocatalytic performances[49] and
536 that a mixture of anatase and rutile showed a more pronounced catalytic effect[50], as observed
537 for PM2 containing 2.5 wt % of rutile TiO_2 microparticles and 2.5 wt % of anatase TiO_2 NPs.
538 Obviously, the increase of the produced •OH radicals at the paint surface with the irradiation
539 time corroborates the increase of the first order decay of xylene after ageing of PM2. In addition
540 to the difference in crystal structure, a carbonaceous coating was well observed by TEM (Figure
541 1b) and SAXS (Figure 2) in the case of the P1 particles which could also reduce the
542 photocatalytic property. A very thin shell of about 0.16nm was also found at the surface of the
543 P2 NPs in the dispersion D2 (Figure 2). This shell might be rather a surface contamination of

544 the NPs than a carbon coating as observed for P1 but its presence could contribute to the
545 dispersion of the NPs in an organic matrix, as for P1 particles which are intentionally coated
546 with a thin carbon layer in order to improve the compatibility between the inorganic particles
547 and the organic matrix of the paint. Indeed, if P2 NPs are agglomerated/aggregated in a solid
548 state (Figure 1d), they look really well dispersed in a liquid media, when observed by cryo-
549 TEM (Figure 1e). Furthermore, only 10% of aggregation was measured by SAXS/SANS when
550 studying D2 dispersion. As the manufacturer uses this dispersion to formulate the PM2 paint,
551 it is expected that P2 NPs would be well dispersed in the paint. However, the SEM observations
552 of PM2 following the weathering step (Figure 3d), indicate that clusters of NPs are visible but
553 also the plastic substrate, which suggests that the dispersion state of the NPs was not good as
554 expected and also that a significant degradation of the organic matrix occurred. The SEM
555 observation and XPS analysis of PM1 and PM2 performed prior and after the weathering
556 revealed a deterioration of the paint surface following the ageing of the paints. Prior to the
557 ageing, the SEM analysis showed a thin layer of organic matrix covering TiO_2 NPs on PM1
558 and PM2 (Figure 3a and Figure 3b). After climatic ageing of the paints, SEM pictures showed
559 only microparticles and NPs of TiO_2 at the surface, indicating the disappearance of the organic
560 matrix for PM1 Q-UV and PM2 Q-UV. The XPS measurements revealed a total disappearance
561 of the peaks related to the organic matrix (C-C and C-H on Figure 4d) for PM2 paint after
562 ageing compared to C1s spectra of PM1 (Figure 4a). These results highlight the total
563 degradation of the PM2 organic matrix compared to PM1. The surface degradation of the PM1
564 paint is probably only due to the UV-irradiation whereas for the PM2, the degradation can be
565 entirely ascribed to the photocatalytic effect induced by the TiO_2 NPs. At the same time, TiO_2
566 signature significantly increases as observed on Ti_2p and O2s XPS spectra of Figure 4 e) and
567 f), in agreement with the SEM observations. A significant difference is observed for the O1s
568 spectra (Figures 4 band Figure 4e) since there is a change in the relative intensity of the C-O*,

O-C=O* peak related to the organic matrix and the O^{2-} peak related to TiO_2 NPs. The disappearance of the organic matrix in the case of PM2 seems to be directly linked to the emission of high levels of the VOCs. The emission of four VOCs is reduced after ageing as the organic matrix completely disappeared. This results also indicates that more TiO_2 NPs are present at the near surface of PM2 aged samples compared to PM1. This accumulation of TiO_2 NPs at the surface allows better removal of xylene and the absence of the organic matrix leads to a high amount of released TiO_2 NPs in the environment. After ageing, TiO_2 NPs can be released in the environment which could affect the workers when sand old paint or when people rub against a painted wall.

The whole process is illustrated on Scheme 1: a) Paint containing TiO_2 NPs is applied on a substrate, VOCs are present in the atmosphere, b) UV irradiations activate the photocatalytic effect of TiO_2 NPs; ambient VOCs are degraded as well as the organic matrix of paint leading to the emission of new VOCs in the air, c) the degradation of the paint leads to TiO_2 NPs accumulation at the surface of the painted walls and a slight friction causes NPs release in the air.

These results shows that the emitted VOCs have a direct link with the organic matrix of the paint. The higher the content of organic composition in the matrix, the more VOCs are created during the irradiation of the paints. In the case of non-reactive paint PM1, a small quantity of VOCs were emitted compared to the PM2 one. P1 micron size particles showed a small photocatalytic efficiency while degrading the organic matrix. As the degradation of the matrix is weak, the same amount of emitted VOCs was observed after aging of PM1 paint. In contrast, the PM2 paint, which contains anatase TiO_2 NPs, induces greater degradation of the organic matrix due to the higher photocatalytic efficiency which in turn leads to greater emission of VOCs prior to aging i.e. before the

disappearance of the organic matrix. After aging, a very small amount of organic matrix was present in the PM2 paint and the concentration of emitted VOCs decreased.

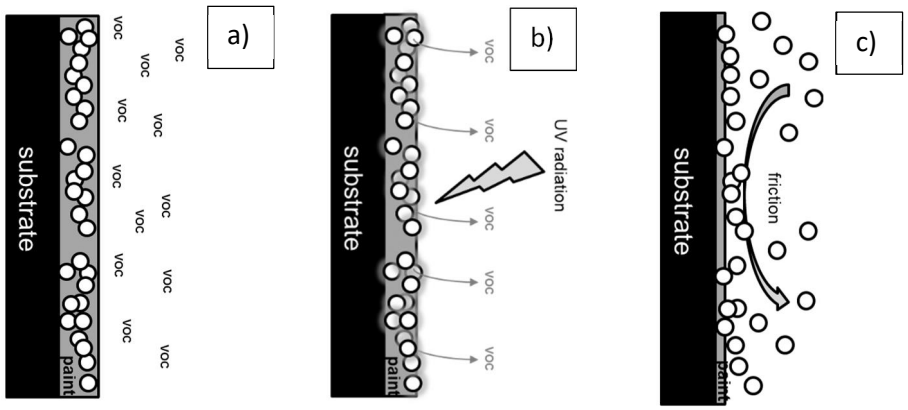

Scheme 1: Simplified illustration of the process leading to emission of new VOCs and release of NPs in the air from the photocatalytic paints.

CONCLUSION

Few studies[20,21,51] have shown that irradiation of the photocatalytic paints leads to generation of VOCs in the air instead of their removal. The origin of these compounds was mainly attributed to the degradation of the organic binder in agreement with our findings. These few studies speculated that the cause of released carbonyl compounds could be the photochemical decomposition of paint binders, without going into deeper systematic investigations.

All these previous studies are based on off-line analytical techniques coupled to the sampling methodology. Thus, the choice of the sampling support and the associated analytical techniques play a crucial role during the identification of the VOCs, beyond the sampling artefacts which can be issued by these methods. This indicates that the selected coupling system (sampling method/analytical technique) will determine the class of detected and identified VOCs. The proton transfer reaction mass spectrometry (PTR-MS)

offers a possibility to observe continuously and on-line a large selection of VOCs with considerably reduced temporal evolution compared to the off-line techniques.

In this study, for the first time to the best of our knowledge, by using the state of the art PTR-ToF-MS instrument we show that the tested photocatalytic paints released organic compounds such as formaldehyde, methanol, acetaldehyde and formic acid upon irradiation.

These results indicate that following only the decaying concentrations of a target compound (in this study xylene) is not sufficient to make an assessment of the effectiveness of photocatalytic paints towards VOCs elimination in various indoor environments. Such an approach does not take into account the fact that stable reaction products, mainly the harmful carbonyls, may occur which can profoundly impact the indoor air quality. These VOCs emerge exclusively from the organic matrix decomposition since much lower emissions were measured in the case of the aged paint which exhibits a lower amount of organic composition in the matrix. In addition, the SEM pictures and XPS analysis indicate that decomposition of the organic matrix induced an accumulation of TiO_2 NPs at the surface of the paint followed by their release in the air. There is no direct relationship between the VOCs emission and the NPs release although both phenomena are caused by the photocatalytic degradation of the organic matrix.

Thanks to the large suite of experiments reported in this paper and the results obtained, different solutions were selected to decrease the release of particles and VOCs in the air and therefore to formulate a ñsafer-by-designò photocatalytic paint. A first approach is to control the degree of the photocatalytic efficiency by modifying the TiO_2 NPs with different coatings and also to control the dispersion state of the NPs in the organic matrix to decrease its degradation while maintaining an optimum photocatalytic efficiency of the paints. The selected coatings should have a good affinity with the organic matrix to have

a good dispersion of the NPs in the paint. Another choice is localization (grafting) of TiO_2 NPs on bigger particles to prevent NPs release and to improve the affinity between NPs and the organic matrix and to reduce the release of NPs. Finally, more resistant binders should be tested to reinforce the organic matrix. All of the suggested solutions are currently under investigation in our laboratory in cooperation with the manufacturer of these paints.

AUTHOR INFORMATION

Corresponding Author

*Phone: +33 (0)4 38 78 08 81; email: delphine.boutry@cea.fr

*Phone: +862085291497; email: gligorovski@gig.ac.cn

Notes

The Authors declare no competing financial interest.

ACKNOWLEDGMENTS:

This work was carried out in the framework of the LABEX SERENADE (ANR-11-LABX-0064) funded by the French Government program, Investissements dôAvenir and managed by the French National Agency (ANR). HR cryo-TEM was funded by the EQUIPEX project ANR-10-EQPX-39-01 called NanoID. We are equally grateful to Frédéric Amblard and Cécile Ducros and Manuel Maréchal for their contribution.

668 REFERENCES:

669 (1) M.J. Hanus, A.T. Harris, *Progress in Materials Science*, 2013, **58**, 1056-1102

670

671 (2) M. Malaki, Y. Hashemzadeh, M. Karevan, *Progress in Organic Coatings*, 2016, **101**, 477-

672 485

673

674 (3) H. Ye, L. Zhu, W. Li, G. Jiang, H. Liu, H. Chen, *Chemical Engineering Journal*, 2017,

675 doi: http://dx.doi.org/10.1016/j.cej.2017.03.088

676

677 (4) E. Ghafari, S.A. Ghahari, Y. Feng, F. Severgnini, N. Lu, *Composites Part B*, 2016, **105**,

678 160-166

679

680 (5) A. Zhang, B. Mu, Z. Luo, A. Wang, *Dyes and Pigments*, 2017, **139**, 473-481

681

682 (6) P. van Broekhuizen, F. van Broekhuizen, R. Cornelissen, L. Reijnders, *J. of Nanopart.*

683 *Res.*, 2011, doi: 10.1007/s11051-010-0195-9

684

685 (7) J. Lee, S. Mahendra, P.J.J. Alvarez, *ACS Nano*, 2010, **4**, 7, 3580-3590

686

687 (8) S.J. Tsai, R.F. Huang, M.J. Ellenbecker. *Ann. Occup. Hyg.*, 2010, **54**, 1, 78-87

688

689 (9) V. Cesard, E. Belut, C. Prevost, A. Taniere, N. Rimbert, *Ann. Occup. Hyg.*, 2013, **57**, 3,

690 345-359

691

(10) C. Brochot, N. Michielsen, S. Chazelet, D. Thomas, *Ann. Occup. Hyg.*, 2012, **56**, 5, 595-605

(11) S.A. Grinshpun, H. Haruta, R.M. Eninger, T. Reponen, R.T. McKay, S.A. Lee, *J. Occ. Env. Hyg.*, 2009, **6**, 10, 593-603

(12) S. Rengasamy, B. Eimer, *Annals of Occupational Hygiene*, 2011, **55**, 3, 253ï 263

(13) L. Vinches, N. Testori, P. Dolez, G. Perron, K.J. Wilkinson, S. Hallé, *Nanoscience Methods*, 2013, **2**, 1, 1-15

(14) Y. Lynch, C. Weiss, E. Valsami-Jones, *Nano Today*, 2014, **9**, 266-270

(15) G. Morose, *J. of Cleaner Production*, 2010, **18**, 285-289

(16) E. Boonen, A. Beeldens, *Coatings*, 2014, **4**, 553-573

(17) C. Toro, B.T. Jobson, L. Haselbach, S. Shen, S.H. Chung, *Atmospheric Environment*, 2016, **139**, 37-45

(18) A.L. da Silva, D.N.F. Muche, S. Dey, D. Hotza, R.H.R. Castro, *Ceramics International*, 2016, **42**, 5113-5122

(19) A. Gandolfo, L. Rouyer, H. Wortham, S. Gligorovski, *Applied Catalysis B: Environmental*, 2017, **209**, 429-436

(20) J. Gunschera, J.R. Andersen, N. Schulz, T. Salthammer, Chemosphere, 2009, **75**, 476-482

(21) T. Salthammer, F. Fuhrmann, *Environ. Sci. Technol.*, 2007, **41**, 6573-6578

(22) M.E. Monge; B. D'Anna, C. George, *Phys. Chem. Chem. Phys.*, 2010, **12**, 8991-8998

(23) A. Gandolfo, V. Bartolomei, E. Gomez Alvarez, S. Tlili, S. Gligorowski, J. Kleffmann, H. Wortham, *Applied. Catalysis. B: Environmental*, 2015, **166-167**, 84-90

(24) A. Al-Kattan, A. Wichser, S. Zuin, Y. Arroyo, L. Golanski, A. Ulrich, B. Nowack, *Environ. Sci. and Tech*. 2014, **48**, 6710-6718

(25) A. Al-Kattan, A. Wichser, R. Vonbank, R.; S. Brunner, A. Ulrich, S. Zuin, B. Nowack, *Environ. Sci. Processes & Impacts*, 2013, **15**, 2186-2193

(26) J. Olabarrieta, S. Zorita, N. Pena, N. Rioja, O. Monzon, P. Benguria, L. Scifo, *Applied Catalysis B: Environmental*, 2012, **123-124**, 182-192

(27) N. Shandilya, O. Le Bihan, C. Bressot, M. Morgeneyer, *Environ. Sci. and Tech*., 2015, **49**, 2163-2170

(28) O. Geiss, C. Cacho, J. Barrero-Moreno, D. Kotzias, *Building and Environment*, 2012, **48**, 107-112

(29) D. Kotzias, O. Geiss, S. Tirendi, J. Barrero-Moreno, V. Reina, A. Gotti, G. Cimino-Reale, B. Casati, E. Marafante, D. Sarigiannis, *Fresenius Environmental Bulletin*, 2009, **18**, 670-681

(30) A.M. Dafni, E. Demetriou, N. Michael, E.I. Tolis, J.G. Bartzis, *Atmospheric Environment*, 2010, **44**, 4388-4395

(31) Th. Zemb, P. Lindner, Eds. Neutron, X-rays and Light. Scattering Methods Applied to Soft Condensed Matter, 1st, ed.; North Holland, 2002

(32) B. Fiorentino, L. Golanski, A. Guiot, J-F. Damlencourt, D. Boutry, *J. Nanopart. Res*, 2015, **17**, 149

(33) A. Fujishima, T.N. Rao, D.A. Tryk, *J. of Photochem. and Photobiol. C: Photochemistry Reviews* 2000, **1**, 1ï 21

(34) R.F. Howe, M. Grätzel, *J. Phys. Chem.*, 1987, **91**, 3906-3909

(35) M. Anpo, M. Che, B. Fubini, E. Garrone, E. Giamello, M.C. Paganini, *Topics in Catalysis*, 1999, **8**, 189-198

(36) C. Naccache, P. Meriaudeau, M. Che, A.J. Tench, *J. Chem. Soc. Faraday Trans.*, 1971, **67**, 506-512

(37) J.M. Coronado, A.J. Maira, J.C. Conesa, K.L. Yeung, V. Augugliaro, J. Soria, *Langmuir*, 2001, **h**, 5368-5374

(38) S-C. Ke, T-C. Wang, M-S. Wong, N.O. Gopal, *J. Phys. Chem. B*, 2006, **110**, 11628-11634

(39) M.D. Sevilla, D. Becker, M. Yan, *J. Chem. Soc. Faraday Trans.*, 1990, **86**, 19, 3279-3286

(40) T. Rajh, A.E. Ostafin, O.I. Micic, D.M. Tiede, M.C. Thurnauer, *J. Phys. Chem.*, 1996, **100**, 4538-4545

(41) Y. Nakaoka, Y. Nosaka, *J. of Photochem. and Photobiol. A: Chemistry*, 1997, **110**, 299-305

(42) C.P. Kumar, N.O. Gopal, M-S. Wang, K.S. Ke, *J. Phys. Chem. B*, 2006, **110**, 5223-5229

(43) M.V. Motyakin, S. Schlick, *Macromolecules*, 2001, **34**, 2854-2864

(44) R. Morelli, I.R. Bellobono, C.M. Chiodaroli, S. Alborghetti, *J. of Photochem. and Photobiol. A: Chemistry*, 1998, **112**, 271-276

(45) T. Salthammer, *International Journal of Hygiene and Environmental Health*. 2015, **218**, 433ï 436.

(46) Y. Gao, H. Wang, J. Wu, R. Zhao, Y. Lu, B. Xin, *Applied Surface Science*, 2014, **294**, 36-41

(47) N. Yuangpho, S.T.T. Le, T. Treerujiraphapong, W. Khanitchaidecha, A. Nakaruk, *Physica E*, 2015, **67**, 18-22

(48) D.C. Hurum, A.G. Agrios, K.A. Gray, T. Rajh, M.C. Thurnauer, *J. Phys. Chem. B*, 2003, **107**, 4545-4549

(49) S. Wang, J.S. Lian, W.T. Zheng, Q. Jiang, *Applied Surface Science*, 2012, **263**, 260-265

(50) L. Zao, M.D. Han, J.S. Lian, *Thin Solid Films*, 2008, **516**, 3394-3398

(51) J. Auvinen, L. Wirtanen, *Atmos. Environ*. 2008, **42**, 18, 4101ï 4112.

TOC Art